INTERNATIONAL JOURNAL OF NUMERICAL MODELLING: ELECTRONIC NETWORKS, DEVICES AND FIELDS
Int. J. Numer. Model. 2009; **22**:57–76
Published online 1 September 2008 in Wiley InterScience (www.interscience.wiley.com). DOI: 10.1002/jnm.698

Efficient power-bus modeling based on an adaptive frequency sampling technique

Giulio Antonini[1,*,†], Dirk Deschrijver[2] and Tom Dhaene[2]

[1]*UAq EMC Laboratory, Dipartimento di Ingegneria Elettrica e dell'Informazione, Università degli Studi di L'Aquila, Monteluco di Roio, 67040 L'Aquila, Italy*
[2]*Department of Information Technology (INTEC), Ghent University-IBBT, Sint Pietersnieuwstraat 41, 9000 Ghent, Belgium*

SUMMARY

This paper presents an adaptive frequency sampling algorithm to generate a rational macromodel of a power delivery network. To this aim, the cavity model is assumed to represent the structure and accurate models of conductor and dielectric losses are incorporated. The adaptive sampling algorithm allows one to minimize the order of the macromodel and number of frequency samples used to extract the rational macromodel. The numerical results demonstrate the effectiveness of the proposed method. Copyright © 2008 John Wiley & Sons, Ltd.

Received 15 December 2007; Revised 23 May 2008; Accepted 7 July 2008

KEY WORDS: power delivery networks; cavity model; rational macromodeling

1. INTRODUCTION

Power delivery networks are used for delivering DC power to integrated circuits (ICs) in multilayer printed circuit boards (PCBs). The DC power-bus structure includes entire planes of large area and is essentially a parallel-plane waveguide [1]. Modes excited within the planes may result in signal integrity (SI) and electromagnetic interference (EMI) problems [2–7].

Full-wave techniques such as the finite-difference time-domain (FDTD) method [8,9], the finite element method [10] or the partial element equivalent circuit (PEEC) approach [5,11] have been widely adopted to obtain accurate models of power-bus structures. Full-wave equivalent circuit models have been proposed in order to allow the fringing fields to be taken into account

*Correspondence to: Giulio Antonini, UAq EMC Laboratory, Dipartimento di Ingegneria Elettrica e dell'Informazione, Università degli Studi di L'Aquila, Monteluco di Roio, 67040 L'Aquila, Italy.
†E-mail: antonini@ing.univaq.it

Contract/grant sponsor: Italian Ministry of University (MIUR); contract/grant number: 2006095890
Contract/grant sponsor: Fund for Scientific Research in Flanders (FWO Vlaanderen)

[12–14]. Despite their accuracy, all these techniques are usually time and memory consuming and their use may be unpractical even for simple geometries.

In the specific case of power delivery networks, the electromagnetic field can be assumed to have a TM structure because of the small thickness of PCBs. Under this hypothesis a full cavity model has been generated to characterize the rectangular power-bus structure as a multiport microwave circuit [15]. Maxwell's equation are re-cast as a second-order differential equations, which admits a Green's function in series form. The spectral representation of Green's function allows the impedance matrix $\mathbf{Z}$ to be expressed as a double infinite series. Such a series is characterized by a slow convergence and requires many terms to obtain an acceptable accuracy. Irregular shapes of the power-bus structure can be modeled by using the segmentation technique [16–18].

The convergence of the double infinite series can be partially improved by reducing it to a single infinite series [19,20], although it may take hundreds or thousands of terms to achieve an acceptable accuracy. The use of fast algorithms [21,22] can significantly accelerate the convergence of the single infinite series.

It is clear that either the full-wave techniques or the cavity model contain more information than really needed and a model-order reduction (MOR) approach is required to capture the behavior of the structure without redundancy, limiting the order of the approximation while preserving accuracy.

The aim of this paper is to present a systematic macromodeling approach of power-bus structures based on the cavity model that is able to capture all resonances and anti-resonances with a minimal workload, hereby selecting a minimal order of the macromodel and minimal number of frequency samples. Since the dominant poles are identified, it allows one to simplify the synthesized SPICE-compatible equivalent circuit. Additionally, the macromodel can be integrated with non-linear models allowing realistic transient analysis.

Finally, the proposed technique is fully compatible with existing numerical techniques to accelerate the computation of the cavity model, meaning that all frequency samples can be computed using the methods presented in [21,22], or using $3D$ methods such as the PEEC method [11] and the finite-difference algorithm [13,14].

2. POWER-BUS MACRO-MODELING

The cavity model proposed in [15] provides an elegant way to compute the impedance matrix of a power bus as a double infinite summation that can be synthesized in a straightforward way. As mentioned above, one concern is related to the fact that such an infinite summation is slowly convergent and this leads to a large number of modes and, thus, of lumped elements in the equivalent circuit. The double infinite series can be cast into a single infinite series [19,20] and its computation made more efficient. More recent acceleration techniques have been proposed in [21–23], allowing to significantly speed-up the computation of all $\mathbf{Z}$ matrix entries. The asymptotic waveform evaluation (AWE) technique has also been applied to the eigenmode expansion in [24]. These acceleration techniques perform an MOR, thus reducing the complexity of the equivalent circuit used for analyzing the simultaneous switching noise on the plane pairs for PCBs or multi-chips modules. All these methods focus on the efficient computation of the impedance matrix but do not face the issue of generating accurate and efficient macromodels for transient analysis.

DOI: 10.1002/jnm

This task requires the following issues to be addressed:

- usage of physically consistent models of conductor and dielectric losses;
- minimization the order of the macromodel and the number of frequency samples.

For a rectangular plane structure with dimensions $a \times b$, separated by a dielectric of thickness $h \ll \lambda_{\min}$ (where $\lambda_{\min}$ is the minimum wavelength over the frequency range of interest) and permittivity ε, the impedance matrix at arbitrary ports on the plane can be computed as [25]

$$\begin{aligned} Z_{ij}(\mathrm{j}\omega) = \sum_{m=0}^{\infty}\sum_{n=0}^{\infty} \frac{\mathrm{j}\omega\mu h C_m C_n}{(k_{mn}^2 - k^2)ab} \\ \times \cos\left(\frac{m\pi x_i}{a}\right)\mathrm{sinc}\left(\frac{m\pi t_{xi}}{2a}\right)\cos\left(\frac{n\pi y_i}{b}\right)\mathrm{sinc}\left(\frac{n\pi t_{yi}}{2b}\right) \\ \times \cos\left(\frac{m\pi x_i}{a}\right)\mathrm{sinc}\left(\frac{m\pi t_{xi}}{2a}\right)\cos\left(\frac{n\pi y_i}{b}\right)\mathrm{sinc}\left(\frac{n\pi t_{yi}}{2b}\right) \end{aligned} \tag{1}$$

$\mathrm{sinc}(x) = \sin(x)/x$, $k_{mn}^2 = (m\pi/a)^2 + (n\pi/b)^2$, m represents the mth mode associated with the x-dimension, n represents the nth mode associated with the y-dimension, (x_i, y_i) are the coordinates of the center of the ith port and (t_{xi}, t_{yi}) are the dimensions of the ith port. The constant $C_m = 1$ if $m = 0$ and $C_m = 2$ if $m \neq 0$ and ω is the angular frequency.

2.1. Improved modeling of conductor and dielectric losses

Originally the complex transverse wave number k^2 was defined as [26]

$$k^2 = (k' - \mathrm{j}k'')^2 = \omega^2\epsilon_0\epsilon_r\mu(1 - \mathrm{j}(\tan\delta + 1/h\sqrt{\pi f\mu\sigma})/2)^2 \tag{2}$$

More recently in [21] the complex transverse wave number k^2 has been defined as

$$k^2 = \omega^2\mu\epsilon - \frac{\mathrm{j}2\omega\epsilon Z_s}{h} \tag{3}$$

where μ and ε denote the permeability and permittivity of the dielectric, respectively, Z_s is the surface impedance of the imperfect conductor of the power/ground planes, given by [27]

$$Z_s = (1 + \mathrm{j})R_s, \quad R_s = \frac{1}{\delta_s\sigma}, \quad \delta_s = \frac{1}{\sqrt{\pi f\mu\sigma}} \tag{4}$$

where R_s is the surface resistivity of the conductor layer, δ_s is the skin depth of field penetration into the conductor and σ is the electrical conductivity.

A broadband macromodel of the power/ground structure requires that phenomena are accurately modeled from DC to the maximum frequency of interest. Model (1) is only accurate above some tens of MHz as it assumes approximate models of both conductor and dielectric losses.

Both models (2) and (3), incorporating frequency-dependent conductor losses, assume that the skin-effect is well developed and loses accuracy as frequency decreases. This is a critical task also for macromodeling purposes.

Furthermore, the lossy and dispersive behavior of dielectrics is usually modeled as

$$\epsilon = \epsilon' - \mathrm{j}\epsilon'\tan\delta \tag{5}$$

DOI: 10.1002/jnm

This model of dielectric losses may be not accurate at low frequencies as it selects $\tan\delta$ at a specific frequency f_{dl}, where polarization losses are significant and then extend the estimate to the entire frequency bandwidth of interest [28]. It is well known that polarization losses are frequency dependent and may become important in the range of hundreds of MHz and vanish at lower frequencies.

In a power-bus structure, electric and magnetic fields propagation is determined by longitudinal and transverse phenomena. In order to build a more rigorous model, firstly we identify the unitary impedance and admittance describing longitudinal and transverse phenomena:

$$Z'(\mathrm{j}\omega) = \left(\frac{2Z_s(\mathrm{j}\omega)}{h} + \mathrm{j}\omega\mu\right) \tag{6a}$$

$$Y'(\mathrm{j}\omega) = \mathrm{j}\omega\epsilon(\mathrm{j}\omega) \tag{6b}$$

The complex transverse wave number can be defined as

$$k^2(\mathrm{j}\omega) = -Z'(\mathrm{j}\omega)\,Y'(\mathrm{j}\omega) \tag{7}$$

Thus, when using the cavity model, losses are accounted for by changing the complex transverse wave number. The consistency of the model, as in transmission lines modeling where conductor losses are described in terms of a longitudinal per unit length resistance, requires that also the longitudinal unitary impedance is changed correspondingly. Thus, the generic **Z** matrix entry (1) can be re-written, in the Laplace domain, as

$$\begin{aligned} Z_{ij}(s) = \sum_{m=0}^{\infty}\sum_{n=0}^{\infty} & \frac{Z'(s)hC_mC_n}{(Z'(s)\,Y'(s)+k_{mn}^2)ab} \\ & \times \cos\left(\frac{m\pi x_i}{a}\right)\mathrm{sinc}\left(\frac{m\pi t_{xi}}{2a}\right)\cos\left(\frac{n\pi y_i}{b}\right)\mathrm{sinc}\left(\frac{n\pi t_{yi}}{2b}\right) \\ & \times \cos\left(\frac{m\pi x_j}{a}\right)\mathrm{sinc}\left(\frac{m\pi t_{xj}}{2a}\right)\cos\left(\frac{n\pi y_j}{b}\right)\mathrm{sinc}\left(\frac{n\pi t_{yj}}{2b}\right), \quad i,j=1,\ldots,N_p \end{aligned} \tag{8}$$

In the present work, impedance $Z_s(\mathrm{j}\omega)$, describing the current distribution in the conductor, is assumed obeying a transverse electromagnetic field (TEM) law. This makes it possible to compute the impedance $Z_s(\mathrm{j}\omega)$ numerically, as detailed in [29]. In fact, at low frequencies the power-bus structure exhibits a capacitive behavior, which might be compromised by a poor model of conductor and dielectric losses.

At low frequencies, the dominant mode is $(m,n)=(0,0)$. If we calculate the limit of $Z_{ij}(s)$ as $s\to 0$, we obtain

$$\lim_{s\to 0} Z_{ij}(s) = \lim_{s\to 0}\frac{Z'(s)h}{Z'(s)\,Y'(s)ab} = \lim_{s\to 0}\frac{h}{Y'(s)ab} = \lim_{s\to 0}\frac{h}{s\epsilon(s)ab}, \quad i,j=1,\ldots,N_p \tag{9}$$

Thus, the low-frequency poles are determined by the zeros of $s\epsilon(s)$: a poor modeling of dielectric losses may result in unstable poles and special care is required to fit the complex permittivity.

A more suitable model of non-ideal dielectrics is based on Debye and Lorentz models, which allows one to describe the lossy and dispersive behavior of dielectrics as

DOI: 10.1002/jnm

$$\epsilon(s) = \epsilon_0 \left[\epsilon_\infty + \sum_{m=1}^{N_D} \frac{(\epsilon_{DS,m} - \epsilon_{D\infty,m})}{1 + s\tau_m} + \sum_{n=1}^{N_L} \frac{(\epsilon_{LS,n} - \epsilon_{L\infty,n})\omega_{0,n}^2}{s^2 + 2s\delta_n + \omega_{0,n}^2} \right] \tag{10}$$

where parameters ϵ_∞, $\epsilon_{DS,m}$, $\epsilon_{D\infty,m}$, $(m = 1, \ldots, N_D)$, $\epsilon_{LS,n}$ and $\epsilon_{L\infty,n}, (n = 1, \ldots, N_L)$ are all positive and satisfy the following conditions:

$$\epsilon_S = \epsilon_0 \left(\sum_{m=1}^{N_D} \epsilon_{DS,m} + \sum_{n=1}^{N_L} \epsilon_{LS,n} \right) \tag{11a}$$

$$\epsilon_\infty = \epsilon_0 \left(\sum_{m=1}^{N_D} \epsilon_{D\infty,m} + \sum_{n=1}^{N_L} \epsilon_{L\infty,n} \right) \tag{11b}$$

As stated above, dielectric permittivity is usually described in terms of the static permittivity ϵ' and loss factor $\tan\delta$, which are obtained by measurements. In order to adopt the rational models based on Debye and Lorentz expansion (10), the parameters ϵ_∞, $\epsilon_{DS,m}$, $\epsilon_{D\infty,m}, (m = 1, \ldots, N_D)$, $\epsilon_{LS,n}$ and $\epsilon_{L\infty,n}, (n = 1, \ldots, N_L)$ need to be recovered.

If wideband measurements are available for the frequency-dependent permittivity, a fitting technique [30] can be adopted to extract a rational approximation of $\epsilon(s)$. Otherwise, if the characteristics of the dielectric are know at a single frequency sample, the method presented in [31] can be used to obtain a reasonable model for lossy and dielectric permittivity.

2.2. Realization

The rational modeling technique described in the following aims to generate a pole–residue macromodel of the power-bus structure using the cavity model while limiting the number of frequency samples and the order of the rational approximation. The vector fitting (VF) technique [30] can be used to build a rational approximation based on the frequency response of a linear system; in the case of the power/ground plane pair the impedance matrix (1) is usually approximated.

In the standard VF technique the order of the macromodel is chosen and fixed upfront; thus, the complexity of the final equivalent circuit is fixed as well. Choosing the order is not obvious for highly resonant structure like power/ground pair planes. On the other hand, higher orders, while providing satisfactory accuracy, easily lead to unnecessary complex equivalent circuits. Furthermore, overfitting may negatively impact the passivity of the generated macromodel as it may increase the probability of outbound passivity violations [32]. Thus, there are at least two reasons to limit the order of the rational approximation. An *a priori* estimation of the model order is not a trivial task. To this aim the adaptive frequency sampling (AFS) algorithm, described in the following section, can be effective.

3. RATIONAL MODELING ALGORITHM

The computation time to build a macromodel of power-bus structures might take so long that one limits the number of data samples in order to get results in a moderate amount of time. If the sampling rate is reduced, undersampling may occur, which means that some important features, such as coupling effects and resonances, may be missed. Even if most of the desired frequency range is oversampled, some important effects can still be missed due to local

DOI: 10.1002/jnm

undersampling [33]. Traditionally, some prior knowledge of the system dynamics is required in order to select an appropriate sample distribution and an appropriate model complexity to accurately represent the impedance matrix of the structure. To alleviate this problem, an efficient rational modeling scheme is applied, which combines the use of VF and AFS.

3.1. Vector fitting

VF is a robust macromodeling tool for rational approximation in the frequency domain. Based on a frequency response, the technique iteratively calculates a suitable set of poles and solves the residues of the transfer function in a two-step procedure, see [30,34] for details. The rational model is generated for the admittance matrix:

$$\mathbf{Y}(\mathrm{j}\omega) = \mathbf{Z}^{-1}(\mathrm{j}\omega) \tag{12}$$

as it can be more easily linked to lumped elements, such as decoupling capacitors, and can be incorporated in SPICE-like solvers that are based on modified nodal analysis (MNA) [35]. During the fitting process, it is ensured that all elements of the admittance matrix share a common set of poles. Based on the partial fraction expansion of the transfer function, the corresponding circuit realization can be easily obtained [36]. A direct application of the inverse Laplace transform yields the following state-space equations:

$$\dot{\mathbf{x}}(t) = \mathbf{A}\mathbf{x}(t) + \mathbf{B}\mathbf{v}(t) \tag{13}$$

$$\mathbf{i}(t) = \mathbf{C}\mathbf{x}(t) + \mathbf{D}\mathbf{v}(t) \tag{14}$$

where $\mathbf{A} \in \Re^{p\times p}$, $\mathbf{B} \in \Re^{p\times q}$, $\mathbf{C} \in \Re^{q\times p}$, $\mathbf{D} \in \Re^{q\times q}$, p is the number of states and q is the number of ports. As the admittance matrix representation is used in this case, the input and output vectors correspond to port voltages $\mathbf{v}(t)$ and port currents $\mathbf{i}(t)$, respectively.

3.2. Adaptive sampling algorithm

An adaptive sampling technique is applied, which automatically selects a limited number of data samples in consecutive iterations, and approximates the data by a rational pole–residue model using the VF technique [37]. At the same time, the order of the rational model is kept minimal [38–40]. Figure 1 shows a flowchart of the algorithm: it consists of an adaptive modeling loop and an adaptive sampling loop. A pseudo-code description of the algorithm is also provided.

3.2.1. Adaptive modeling loop. The algorithm starts with a set of four data samples that are equidistantly spread over the frequency range of interest. Depending on the number of available data points, multiple rational fitting models are built with different orders of numerator and denominator, exploiting all degrees of freedom. The RMS error of all fitting models is calculated, and all models are rated and ranked accordingly. If the RMS error between the best calculated fitting models and the selected data points exceeds a predefined threshold, then the models are rejected and the model complexity is increased.

3.2.2. Adaptive sampling loop. Once the selected data samples are approximated sufficiently well, the most accurate fitting models are selected and compared by a set of heuristical rules, which are reported in [41]. Such rules provide an error estimate that can be used to validate the quality of the overall models [42]. If the estimated error of the models is too high, due to an inaccurately frequency response, then the adaptive sampling loop will select additional data

DOI: 10.1002/jnm

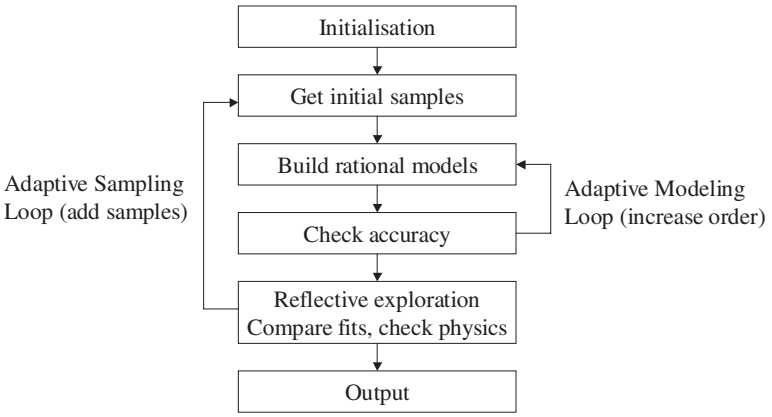

Figure 1. Flowchart of the AFS algorithm.

Table 1. Parameters of the power bus.

Conductor plane (cm)			Port location (cm)				Dielectric properties	
			Port 1		Port 2			
a	b	h	x_1	y_1	x_2	y_2	ϵ_r	tan
26.5	20.7	0.1	4.7	4.7	8.5	8.5	4.5	0.02

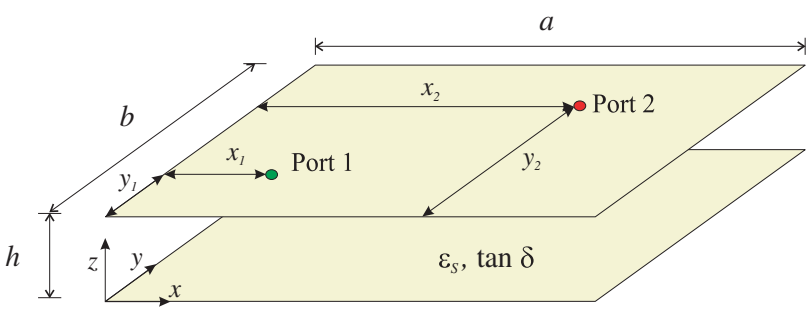

Figure 2. Schematic of a two-layer power-bus structure (Example 1).

samples at well-chosen frequency locations, and afterwards the adaptive modeling loop will update the rational fitting models. The location of new frequency samples is determined by minimizing the maximum relative fitting errors of the best models with respect to the frequency. This process, called reflective exploration [42], is iteratively repeated until the largest mismatch of the response is below a predefined tolerance level.

3.3. Rational model validation

In a final step, two additional data samples can be computed to validate the model. The location of these data samples can be chosen where the estimated fitting error is maximal (error-based

DOI: 10.1002/jnm

sampling), or where the distance between successive data samples is maximal (density-based sampling). These validation samples are typically not used to build the fitting model, unless they indicate premature convergence of the algorithm. When the algorithm is finished, a step-wise reduction of the order using relaxed vector fitting (RVF) [43] can be applied to avoid small redundancies in the model. To ensure stability of the time-domain simulations, passivity of the macromodel is enforced as a post-processing step [32].

Input: Generator of data $Y_{ij}(j\omega)$, Frequency range $[f_{min}, f_{max}]$
Output: State-space model $SER = (A, B, C, D)$
Calculate 4 equidistant data samples $S = \{Y(s_{min}), ..., Y(s_{max})\}$

$convergence = false$;
while $convergence = false$ **do**

  %Adaptive Modeling Loop
  $order\_found = false$;
  while $order\_found = false$ **do**
    foreach *number of poles* $n_{min} < n_p < n_{max}$ **do**
      foreach *number of zeros* $n_{p-1} \leq n_z \leq n_{p+1}$ **do**
        $[SER_i, rmserr_i] = vectfit(S, n_p, n_z)$;
      end
    end
    $[SER_1, rmserr_1] = select\_best(SER_i, rmserr_i)$;
    $[SER_2, rmserr_2] = select\_2nd\_best(SER_i, rmserr_i)$;
    if $rmserr_1 > \delta$ *or* $rmserr_2 > \delta$ **then**
      $n_{min} = n_{min} + 1, n_{max} = n_{max} + 1$;
    else
      $order\_found = true$;
    end
  end

  $[resp_1] = freqresp(SER_1, [f_{min}, f_{max}])$;
  $[resp_2] = freqresp(SER_2, [f_{min}, f_{max}])$;

  %Adaptive Sampling Loop
  $heuristics\_ok = true$;
  foreach *heuristical rule* H_i **do**
    while $heuristics\_ok = true$ **do**
      $heuristics\_ok = heuristics_i(resp_1, resp_2)$;
    end
  end
  if $heuristics\_ok = true$ **then**
    $convergence = true$;
  else
    $s_{new} = getfreq(\max_s(|resp_1 - resp_2|/|resp_1|))$;
    $Y(s_{new}) = calculate\_data(s_{new})$;
    $S = S \cup Y(s_{new})$
  end

end

$SER = reduce\_order(SER_1)$;
$SER = make\_passive(SER)$;

Algorithm 1. Adaptive frequency sampling (AFS) algorithm.

DOI: 10.1002/jnm

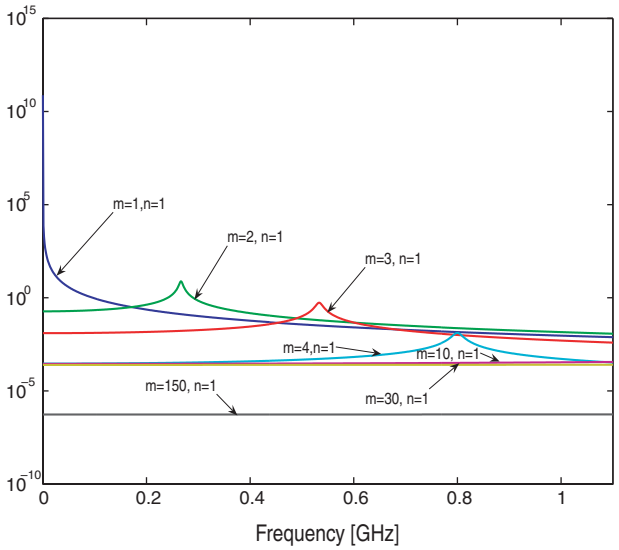

Figure 3. Magnitude spectra of some of modal impedances of Z_{11} (Example 1).

4. VALIDATION STUDIES

4.1. Example 1

In the first example a typical power-bus structure is considered. Figure 2 shows the model geometry and the parameters are summarized in Table 1.

In this example the power-bus structure has been modeled as a planar circuit with two external observation ports with dimensions $t_x = t_y = 0.1$ mm. The method described in [31] has been used to generate the rational representation of the electrical permittivity, matching the experimental data for FR4 ($\epsilon_r = 4.7$ at DC, $\tan\delta = 0.02$ at 100 MHz).

The proper number of modes has been identified by progressively increasing the number to 150. However, it is not computationally efficient to calculate the cavity model with a large number of modes, especially in the case of a large number of ports, because this results into a complex equivalent circuit. As stated in Section 2, not all the modes have the same impact on the overall summation in the frequency band of interest and many of them can be discarded without affecting the accuracy. Figure 3 shows some of the modal impedance modes of Z_{11}.

In order to reduce the computational workload, the proposed AFS method is used. Figures 4 and 5 show a comparison of magnitude and phase spectra of Y_{11} and Y_{12} as obtained by using the proposed AFS technique and by using different numbers of modes $N_x = N_y = 41, 100, 150$. The overall RMS error of the macromodel corresponds to 10^{-4}, which shows that the response of the AFS model corresponds quite well with the reference case obtained with $N_x = N_y = 150$. Note that lower-order cavity models (50 100) are affected by significant errors.

It is also worth mentioning that the AFS macromodel has been generated by adaptively selecting only 30 frequency data samples. Figures 6 and 7 show the spectra of the transfer admittance Y_{11} and Y_{12} computed using a frequency sweep with 1000 samples [15] (solid line)

DOI: 10.1002/jnm

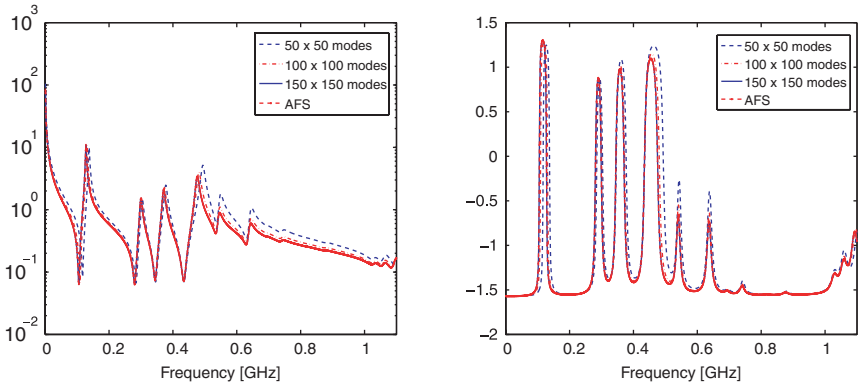

Figure 4. Magnitude spectra of Y_{11} (Example 1). Left: magnitude; right: phase.

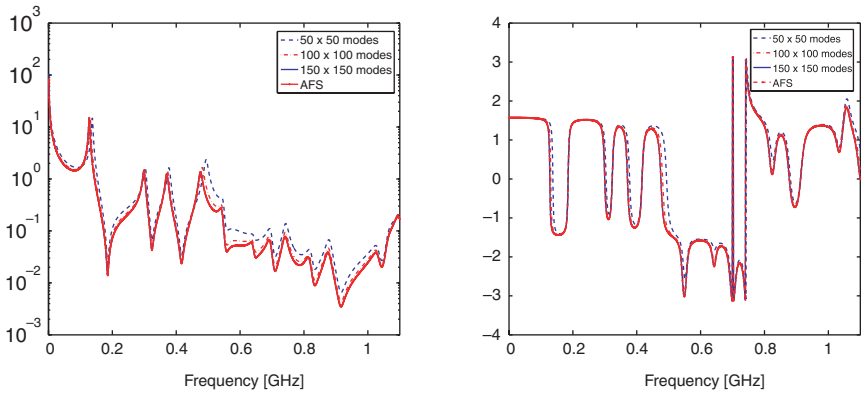

Figure 5. Magnitude spectra of Y_{12} (Example 1). Left: magnitude; right: phase.

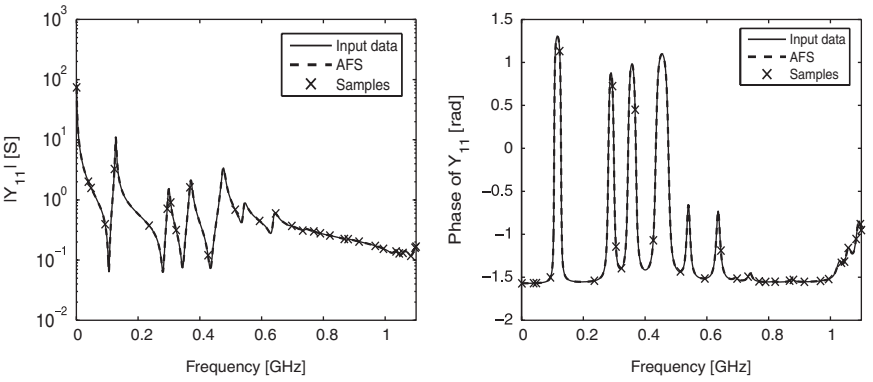

Figure 6. Frequency sampling of Y_{11} (Example 1). Left: magnitude; right: phase.

DOI: 10.1002/jnm

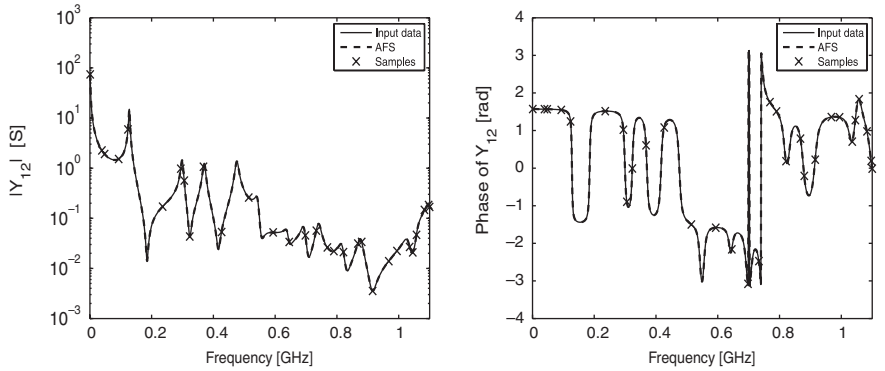

Figure 7. Adaptive frequency sampling of Y_{12} (Example 1). Left: magnitude; right: phase.

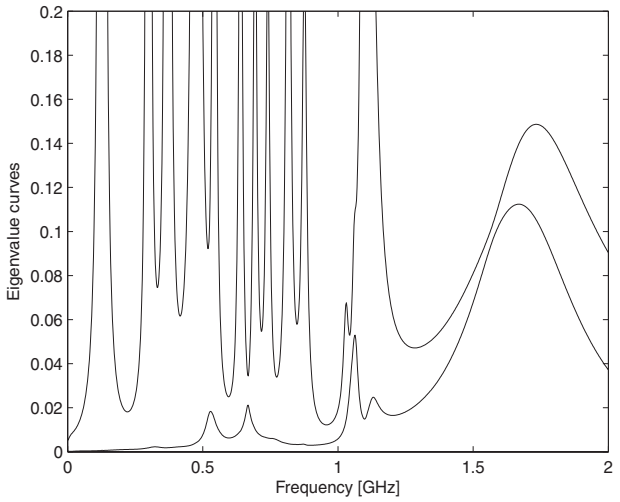

Figure 8. Eigenvalues versus frequency of Real($\mathbf{Y}(j\omega)$) (Example 1).

and the AFS model (dashed line) based on 30 adaptively chosen key frequency samples (crosses): both curves are superimposed.

If we assume that each of the $N_x \times N_y$ modes corresponds to a complex pair and that each complex pair is synthesized by an equivalent circuit with four lumped elements, the total number of circuit elements is $N_{ce} = N_x \times N_y \times 4 = 150 \times 150 \times 4 = 90\,000$. The AFS-based macromodel consists of 36 poles and can be synthesized by an equivalent circuit with only a few hundreds lumped elements.

Passivity of the macromodel can be verified by inspecting the eigenvalues of an associated Hamiltonian matrix. Figure 8 shows a frequency sweep of Real($\mathbf{Y}(j\omega)$) up to 2 GHz, indicating that the macromodel is also passive outside the frequency range of interest. The time-domain

DOI: 10.1002/jnm

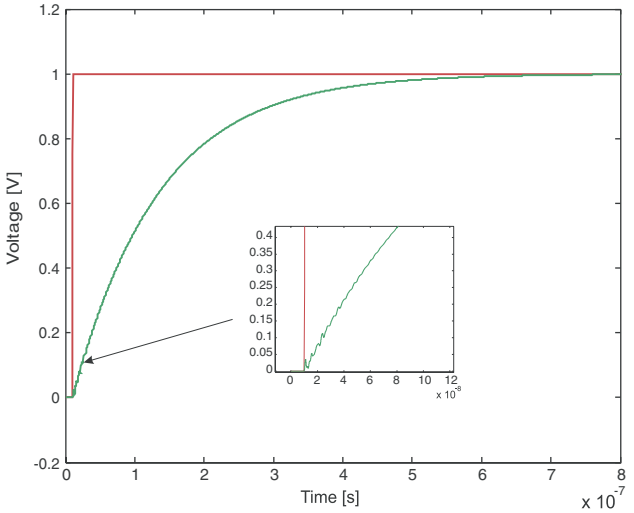

Figure 9. Step response (Example 1).

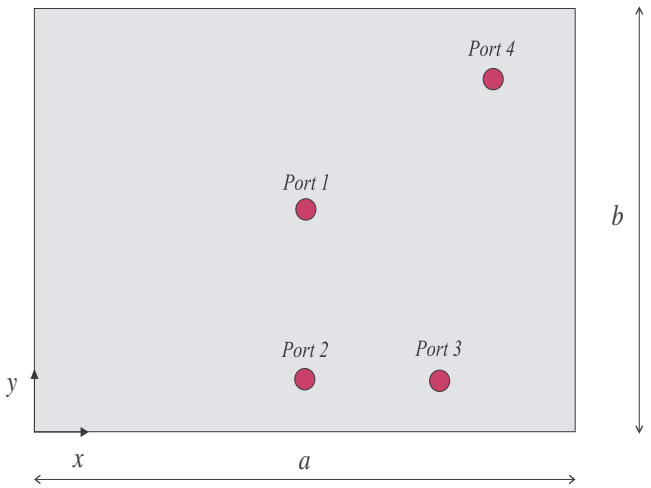

Figure 10. Top view of power/ground structure (Example 2).

step response is also computed: Figure 9 depicts the voltage at port 2 when port 1 is excited by an unitary step with a 1 ns rise time. The causality is strictly preserved, as can be clearly seen.

4.2. Example 2

In the second example we consider a rectangular power-bus structure consisting of two parallel copper planes whose width and length are $W = 254$ mm and $L = 304.8$ mm, respectively. Figure 10 shows the top-view of the structure and the location of the four electrical ports that

DOI: 10.1002/jnm

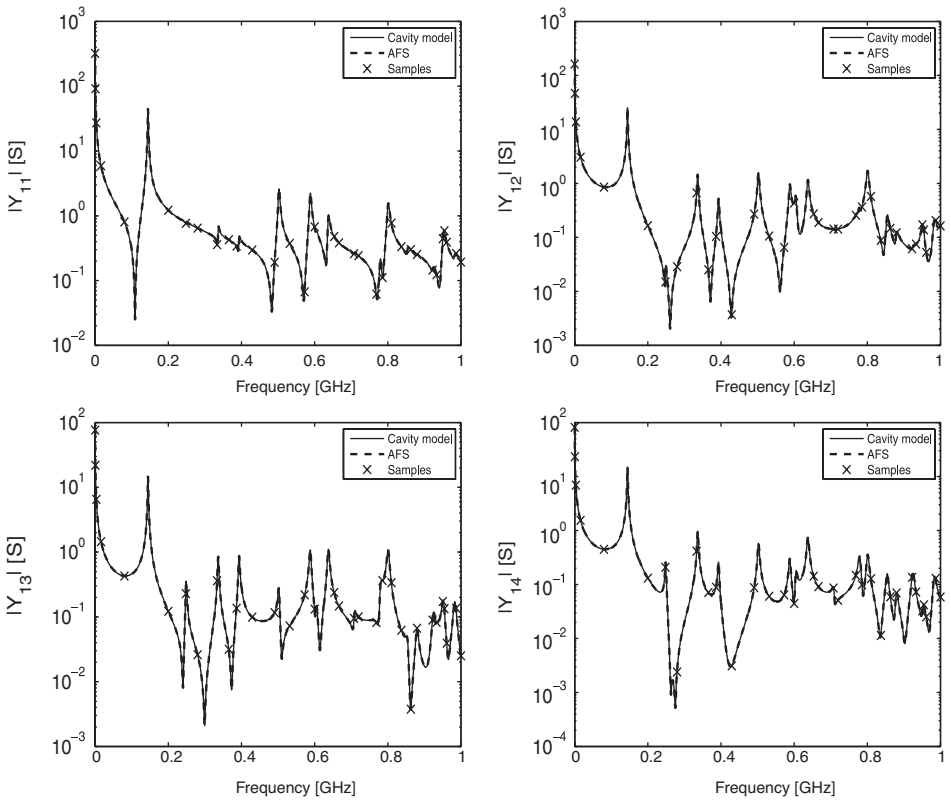

Figure 11. Magnitude spectra of admittances $Y_{1,j}, j = 1, \ldots, 4$ (Example 2).

are located at (152.4 mm, 127 mm), (152.4 mm, 25.4 mm), (228.6 mm, 25.4 mm) and (279.4 mm, 228.6 mm), respectively, with dimensions $t_x = t_y = 0.1$ mm. The dielectric material between the two copper planes has a thickness 1.0161 mm, a relative permittivity of 4.5 and a loss tangent of 0.005.

The reference results are generated by using the cavity model with $N_x = N_y = 100$ in the frequency range 0 Hz-1 GHz, with a frequency spacing of 250 kHz (which means that 4001 equidistant samples are computed). The AFS algorithm automatically calculates a macromodel using only 33 data samples. Inverse magnitude weighting was applied to obtain good approximation of the response at the lower frequencies. The 44-pole macromodel generated by AFS is accurate as confirmed by Figure 11 where the magnitude spectra of admittances $Y_{1j}, j = 1, \ldots, 4$, as evaluated by using the standard cavity model (solid line) and the reduced-order macromodel (dashed line), are compared. No significant difference can be observed, since the RMS error corresponds to 10^{-3} and both curves are again superimposed.

It is known that the unloaded power/ground structure behaves like a capacitor at low frequencies. The low-frequency behavior is significantly affected by the models used for conductor and dielectric losses. Figure 12 shows the phase of impedance Z_{11} using the newly

DOI: 10.1002/jnm

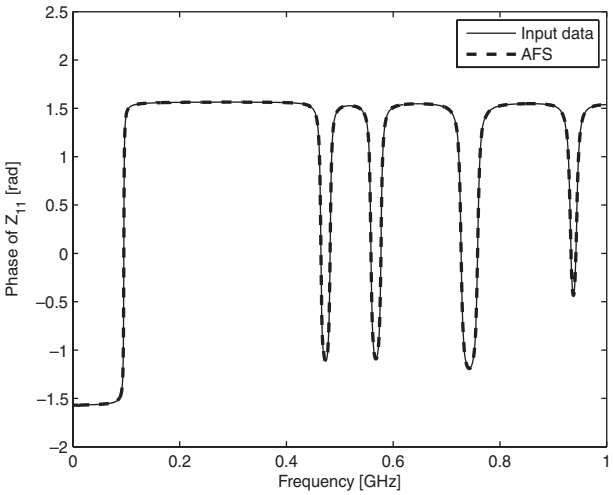

Figure 12. Phase spectrum of impedance Z_{11} (Example 2).

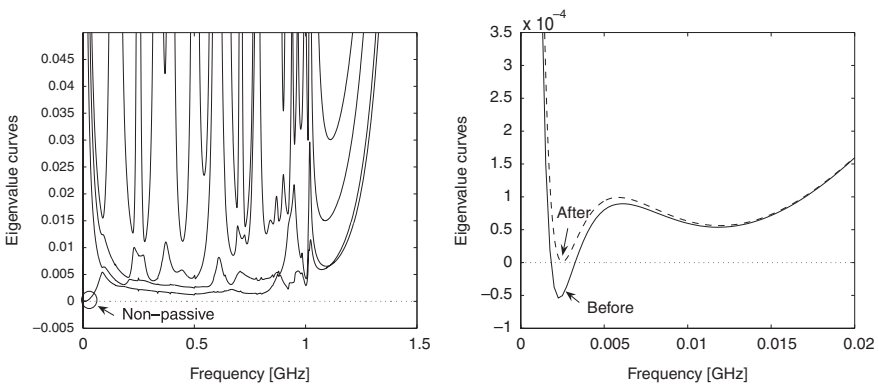

Figure 13. Eigenvalues versus frequency of Real($\mathbf{Y}(j\omega)$) (Example 2). Left panel: full spectrum; right panel: detail of the passivity violation and compensation, at low frequencies.

proposed accurate loss model. As expected, the capacitive behavior is correctly captured at low frequencies, down to DC.

Stability and passivity of the macromodel are crucial to accurately perform a transient analysis and to estimate the voltage bounce correctly. The stability of the macromodel can easily be enforced by flipping all poles in the left half complex plane. Regarding the passivity, the eigenvalue spectrum of Real($\mathbf{Y}(j\omega)$) of the reduced-order macromodel has been computed to detect passivity violations at frequencies, where the eigenvalues are less than zero. Only a minor passivity violation has been detected at low frequencies, which can be easily compensated using the algorithm presented in [32]. Figure 13 shows the eigenvalue spectrum of Real($\mathbf{Y}(j\omega)$) before and after passivity enforcement and a zoom at low frequencies, where the passivity violation has

DOI: 10.1002/jnm

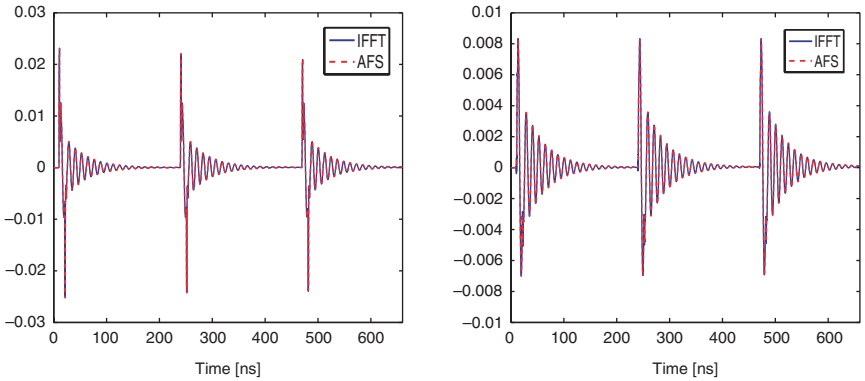

Figure 14. Port voltages (Example 2). Left panel: port 1; right panel: port 4.

been detected. Since the passivity violation is quite small, the compensation does not impact the overall accuracy of the macromodel.

The final macromodel can be either synthesized into an equivalent circuit [44] and implemented in a SPICE-like solver [45] or converted into a state-space realization [36] and simulated by means of an ordinary differential equations (ODEs) solver.

In Figure 14, the transient analysis has been calculated twice: firstly in the frequency domain using the exact admittances and then transformed into the time domain using the IFFT, and secondly, directly in the time domain by using the proposed reduced-order macromodel (AFS). The source voltage is represented by a trapezoidal pulse train with rise and fall times $\tau_r = \tau_f = 1\text{ns}$, pulse width $w = 10\,\text{ns}$, and period $T = 220\,\text{ns}$. Ports 1, 3 and 4 are terminated on $50\,\Omega$ resistances while port 2 is loaded with a decoupling capacitor $C_l = 10\,\mu\text{F}$. Figure 14 shows the results that exhibit good agreement, confirming the robustness of the proposed method to capture the phenomena of power/bus structures.

In order to check the accuracy of the reduced-order model, the feature selective validation (FSV) procedure has been applied. The FSV techniques aims to perform the comparison of different data sets by mimic the behavior of a group of experienced engineers when they perform such a comparison by means of a visual approach [46–48]. The FSV method is based on the decomposition of the original data into two parts: amplitude (trend/envelope) data and feature data. The former component accounts for the slowly varying data across the data set and the latter accounts for the sharp peaks and troughs often found in numerical and experimental data. The numerical figures of merit obtained as output from the FSV procedure can be converted in a natural language descriptor (excellent, very good, good, fair, poor, very poor comparison). The essential meaning of the FSV figures of merit are: ADM (amplitude difference measure), FDM (feature difference measure) and GDM (global difference measure).

The input data are compared with those obtained from the AFS-based macromodel over the frequency range 0–1 GHz. Figure 15 shows the FSV comparison of the magnitude of Y_{14} matrix entry. As seen, all the figures of merit confirm that the AFS model perfectly captures the physics of the system and provides a very good approximation over the entire frequency band 0–1 GHz.

DOI: 10.1002/jnm

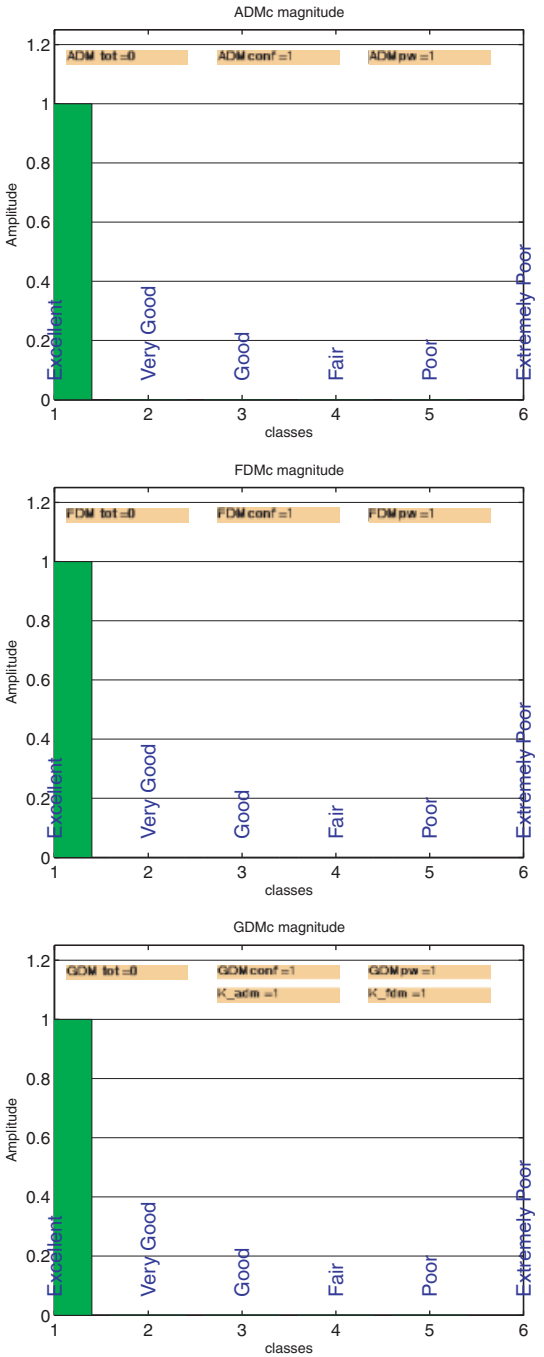

Figure 15. ADMc, FDMc GDMc confidence histograms.

DOI: 10.1002/jnm

5. CONCLUSIONS

In this paper, the AFS technique [38], along with the VF method [30], has been used to generate broadband macromodels of power/ground plane pairs. The proposed approach allows one to automatically generate an accurate passive rational pole–residue approximation of the cavity model over the frequency range of interest. The AFS algorithm limits the order of the macromodel and, as a consequence, simplifies the equivalent circuit of the power-bus structure. Standard passivity enforcement techniques can be used in a post-processing step, as needed. The numerical examples confirm the robustness of the proposed approach to generate accurate and passive SPICE-compatible models, which can be used to evaluate transient voltage bounce due to the simultaneous switching noise.

Finally, it is worth to mention that, although the cavity model has been adopted to extract the **Z** matrix in this paper, any kind of 3D full-wave approach can also be used in conjunction with the AFS technique.

ACKNOWLEDGEMENTS

This work is supported by the Italian Ministry of University (MIUR) under a Program for the Development of Research of National Interest, contract/grant number: PRIN grant-2006095890 and the Fund for Scientific Research in Flanders (FWO Vlaanderen).

REFERENCES

1. Balanis CA. *Antenna Theory: Analysis and Design*. Wiley: New York, 2005.
2. Vaidyanath A, Thoroddsen B, Prince KL, Cangellaris AC. Simultaneous switching noise: influence of plane-ground and plane-signal trace coupling. *IEEE Transactions on Components Packaging and Manufacturing Technology Part A* 1995; **18**(4):496–502.
3. Hall SH, Hall GW, McCall JA. *High-speed Digital System Design—A Handbook of Interconnect Theory and Design Practices*. Wiley: New York, 2000.
4. Yang X-P, Li Z-F. An efficient time-domain macromodel for power/ground bounce analysis. *Microwave and Optical Technology Letters* 2001; **28**(2):224–226.
5. Archembeault B, Ruehli A. Analysis of power/ground-plane EMI decoupling performance using the partial-element equivalent circuit technique. *IEEE Transactions on Electromagnetic Compatibility* 2001; **43**(4): 437–445.
6. Fan JF, Shi H, Orlandi A, Knighten JL, Drewniak JL. Modeling DC power-bus structures with vertical discontinuities using a circuit extraction approach based on a mixed-potential integral equation formulation. *IEEE Transactions on Advanced Packaging* 2001; **24**:143–157.
7. Huang C-C. Circuit modeling of power/ground plane structures for printed circuit boards. *Microwave and Optical Technology Letters* 2005; **47**(1):97–99.
8. Yee KS. Numerical solution of initial boundary value problems involving Maxwell's equations in isotropic media. *IEEE Transactions on Antennas and Propagation* 1966; **14**(5):302–307.
9. Ye X, Koledintseva MY, Li M, Drewniak JL. DC power-bus design using FDTD modeling with dispersive media and surface-mount technology components. *IEEE Transactions on Electromagnetic Compatibility* 1995; **43**(4):579–587.
10. Jin JM. *The Finite Element Method in Electromagnetics* (2nd edn). Wiley: New York, 2002.
11. Ruehli AE, Brennan PA. Efficient capacitance calculations for three-dimensional multiconductor systems. *IEEE Transactions on Microwave Theory and Techniques* 1973; **21**(2):76–82.
12. Fung LC, Leung SW, Wan L, Siu YM, Chen KH. Investigation of ground bounce effect on PCBs. *Microwave and Optical Technology Letters* 2002; **32**(4):259–264.
13. Engin AE, Bharath K, Swaminathan M, Cases M, Mutmury B, Pham N, de Araujo DN, Matoglu E. Finite-difference modeling of noise coupling between power/ground planes in multilayered packages and boards. *Proceedings of Electronic Components and Technology Conference*, San Diego, CA, USA, May 2006.

DOI: 10.1002/jnm

14. Sun S, Pommerenke D, Drewniak J, Xiao K, Chen S-T, Wu T-L. Characterizing package/PCB PDN interactions from a full-wave finite difference formulation. *Proceedings of the IEEE International Symposium on Electromagnetic Compatibility*, Portland, OR, August 2006.
15. Lei GT, Techentin RW, Gilbert BK. High-frequency characterization of power/ground-plane structures. *IEEE Transactions on Microwave Theory and Techniques* 1999; **47**(2):562–569.
16. Okoshi T, Uehara Y, Takeuchi T. The segmentation method-an approach to the analysis of microwave planar circuits. *IEEE Transactions on Microwave Theory and Techniques* 1976; **24**(10):662–668.
17. Sorrentino R. Planar circuits, waveguide models and segmentation method. *IEEE Transactions on Microwave Theory and Techniques* 1985; **33**(10):1057–1066.
18. Wang ZL, Wada O, Toyota Y, Koga R. Modeling of gapped power bus structures for isolation using cavity modes and segmentation. *IEEE Transactions on Electromagnetic Compatibility* 2005; **47**(2):210–218.
19. Richards WF, Lo YT. Theoretical and experimental investigation of a microstrip radiation with multiple lumped linear loads. *Electomagnetics* 1983; **3**(3–4):371–385.
20. Benalla A, Gupta KC. Faster computation of z-matrices for rectangular segments in planar micostrip circuits. *IEEE Transactions on Microwave Theory and Techniques* 1986; **34**:733–736.
21. Wang ZL, Wada O, Toyota Y, Koga R. Convergence acceleration and accuracy improvement in power bus impedance calculation with a fast algorithm using cavity modes. *IEEE Transactions on Electromagnetic Compatibility* 2005; **47**(1):2–9.
22. Liu P, Li Z-F. An efficient method for calculating bounces in the irregular power/ground plane structure with holes in high-speed PCBs. *IEEE Transactions on Electromagnetic Compatibility* 2005; **47**(4):889–898.
23. Wang C, Mao J, Selli G, Luan S, Zhang L, Fan J, Pommerenke DJ, DuBroff DJ, Drewniak JL. An efficient approach for power delivery network with closed-form expressions for parasitic interconnect inductances. *IEEE Transactions on Advanced Packaging* 2006; **29**(2):320–334.
24. Liu P, Li Z-F, Han G-B. Application of asymptotic waveform evaluation to eigenmode expansion method for analysis of simultaneous switching noise in printed circuit boards (pcbs). *IEEE Transactions on Electromagnetic Compatibility* 2006; **48**(3):485–492.
25. Okoshi T. *Planar Circuits for Microwaves and Lightwaves*. Springer: Berlin, 1985.
26. Okoshi T, Miyoshi T. The planar circuit—an approach to microwave integrated circuitry. *IEEE Transactions on Microwave Theory and Techniques* 1972; **20**(4):245–252.
27. Ramo S, Whinnery JR, Van Duzer T. *Fields and Waves in Communication Electronics*. Wiley: New York, 1994.
28. Coperich AK, Cangellaris AC, Ruehli AC. Rigorous modeling of the frequency dependence of ohmic losses in high-speed electrical interconnections. *Proceedings of the IEEE International Symposium on Electromagnetic Compatibility*, Washington, DC, August 2000.
29. Antonini G, Ruehli AE. Combined loss mechanism and stability model for the partial element equivalent circuit technique. *Proceedings of Applied Computational Electromagnetics Conference*, Verona, Italy, March 2007.
30. Gustavsen B, Semlyen A. Rational approximation of frequency domain responses by vector fitting. *IEEE Transactions on Power Apparatus and Systems* 1999; **14**(3):1052–1061.
31. Engin AE, Mathis W, John W, Sommer G, Reichl H. Time domain modeling of lossy substrates with constant loss tangent. *Sixth IEEE Workshop on Signal Propagation on Interconnects*, Heidelberg, Germany, May 2004; 151–154.
32. Saraswat D, Achar R, Nakhla MS. Global passivity enforcement algorithm for macromodels of interconnect subnetworks characterized by tabulated data. *IEEE Transactions on Very Large Scale Integration Systems* 2005; **13**(7):819–832.
33. Burke G, Miller E, Chakrabarti S, Demarest K. Using model-based parameter estimation to increase the efficiency of computing electromagnetic transfer functions. *IEEE Transactions on Magnetics* 1989; **25**: 2807–2809.
34. Deschrijver D, Haegeman B, Dhaene T. Orthonormal vector fitting: a robust macromodeling tool for rational approximation of frequency domain responses. *IEEE Transactions on Advanced Packaging* 2007; **22**(6):504–509
35. Ho C, Ruehli A, Brennan P. The modified nodal approach to network analysis. *IEEE Transactions on Circuits and Systems* 1975; **22**(6):504–509.
36. Kailath T. *Linear Systems*. Prentice-Hall: Englewood Cliffs, NJ, 1980.
37. Antonini G, Deschrijver D, Dhaene T. Adaptive building of accurate and stable PEEC models for EMC applications. *Proceedings of EMC Europe 2006 Symposium*, Barcelona, Spain, September 2006; 51–56.
38. Dhaene T, Ureel J, Faché N, De Zutter D. Adaptive frequency sampling algorithm for fast and accurate S-parameter modeling of general planar structures. *IEEE International Microwave Symposium* 1995, MTT-S 1995, Orlando, FL, 1995; 1427–1430.
39. Dhaene T. Automated fitting and rational modeling algorithm for EM-based S-parameter data. *Sixth International Conference on Applied Parallel Computing* (*PARA 2002*), Springer Lecture Notes in Computer Science, vol. 2367. Espoo, Finland, May 2002; 99–105.

DOI: 10.1002/jnm

40. Deschrijver D, Dhaene T. Efficient GA-inspired macro-modeling of general LTI multi-port systems. *Eighth IEEE Workshop on Signal Propagation on Interconnects*, *SPI 2004*, Heidelberg, Germany, 2004; 95–98.
41. Antonini G, Deschrijver D, Dhaene T. Broadband rational macromodeling based on the adaptive frequency sampling algorithm and the partial element equivalent circuit method. *IEEE Transactions on Electromagnetic Compatibility* 2008; **50**(1):128–137.
42. Beyer U, Smieja F. Data exploration with reflective adaptive models. *Computational Statistics and Data Analysis*. Elsevier Science Publications B.V., Amsterdam, The Netherlands, 1996; 193–211.
43. Gustavsen B. Improving the pole relocating properties of vector fitting. *IEEE Transactions on Power Delivery* 2006; **21**(3):1587–1592.
44. Antonini G. Spice compatible equivalent circuits of rational approximation of frequency domain responses. *IEEE Transactions on Electromagnetic Compatibility* 2003; **45**(3):502–512.
45. Nagel LW. SPICE: A computer program to simulate semiconductor circuits. *Electronics Research Laboratory Report ERL M520*, University of California, Berkeley, May 1975.
46. Duffy A, Martin A, Antonini G, Orlandi A, Ritota C. The feature selective validation (FSV) method. *Proceedings of the IEEE International Symposium on Electromagnetic Compatibility*, Chicago, IL, U.S.A., August 2005.
47. Duffy A, Martin A, Orlandi A, Antonini G, Benson TM, Woolfson M. Feature selective validation (FSV) for validation of computational electromagnetics (CEM). Part I—the FSV method. *IEEE Transactions on Electromagnetic Compatibility* 2006; **48**(2):449–459.
48. Duffy A, Martin A, Orlandi A, Antonini G, Benson TM, Woolfson M. Feature selective validation (FSV) for validation of computational electromagnetics (CEM). Part II—numerical verification. *IEEE Transactions on Electromagnetic Compatibility* 2006; **48**(2):460–469.

AUTHORS' BIOGRAPHIES

Giulio Antonini received the Laurea degree (summa cum laude) in Electrical Engineering in 1994 from the University of L'Aquila and the PhD degree in Electrical Engineering in 1998 from the University of Rome 'La Sapienza'. Since 1998 he has been with the *UAq EMC Laboratory*, Department of Electrical Engineering of the University of L'Aquila where he is actually tenured Associate Professor. His research interests focus on EMC analysis, numerical modeling and in the field of signal integrity for high-speed digital systems. He has authored or co-authored more than 120 technical papers, Three book chapters and given nine keynote lectures at international conferences. He has been the recipient of the IEEE Transactions on Electromagnetic Compatibility Best Paper Award in 1997, the CST University Publication Award in 2004, the IBM Shared University Research Award in 2004, 2005 and 2006; in 2006 he has received a Technical Achievement Award from the IEEE EMC Society 'for innovative contributions to computational electromagnetic on the Partial Element Equivalent Circuit (PEEC) technique for EMC applications'. He holds one European Patent. Since 1998 he collaborates with the IBM T. J. Watson Research Center (New York) in the development of algorithms for PEEC modeling. Prof. Antonini is a member of the TC-9 committee of the IEEE EMC Society and Vice-Chair of the TC-10 Committee of the same IEEE Society. He is in the Technical Program Committee of the Date-06 Conference and serves as reviewer in a number of IEEE journals.

DOI: 10.1002/jnm

Tom Dhaene was born in Deinze, Belgium, on 25 June 1966. He received the PhD degree in Electrotechnical Engineering from the University of Ghent, Ghent, Belgium, in 1993. From 1989 to 1993, he was Research Assistant at the University of Ghent, in the Department of Information Technology, where his research focused on different aspects of full-wave electro-magnetic circuit modeling, transient simulation, and time-domain characterization of high-frequency and high-speed interconnections. In 1993, he joined the EDA company Alphabit (now part of Agilent). He was one of the key developers of the planar EM simulator ADS Momentum. Since September 2000, he has been a Professor in the Department of Mathematics and Computer Science at the University of Antwerp, Antwerp, Belgium. Since October 2007, he is a Full Professor in the Department of Information Technology (INTEC) at Ghent University, Ghent, Belgium. As author or co-author, he has contributed to more than 100 peer-reviewed papers and abstracts in international conference proceedings, journals and books. He is the holder of two US patents.

Dirk Deschrijver was born in Tielt, Belgium, on 26 September 1981. He received the Master degree (licentiaat) and PhD degree in Computer Science in 2003 and 2007, respectively, from the University of Antwerp in Antwerp, Belgium. During the period from 2005 to May October 2005, he was as a Marie Curie Fellow in the Scientific Computing group at the Eindhoven University of Technology in Eindhoven, The Netherlands. Since November 2007, he has been working as a postdoctoral researcher in the Department of Information Technology (INTEC) at Ghent University in Belgium. He is now a Postdoctoral Fellow of the Fund for Scientific Research in Flanders (FWO Vlaanderen). His research interests include robust parametric macromodeling, rational least-squares approximation, orthonormal rational functions, system identification and broadband macromodeling techniques.

DOI: 10.1002/jnm